INSTITUTE OF PHYSICS PUBLISHING BIOINSPIRATION & BIOMIMETICS

Bioinsp. Biomim. **1** (2006) 52–61 doi:10.1088/1748-3182/1/2/003

Active articulation for future space applications inspired by the hydraulic system of spiders

C Menon[1] and C Lira[2]

[1] Advanced Concepts Team, European Space Agency, ESTEC, Keplerlaan 1, 2201 AZ Noordwijk, The Netherlands
[2] Centre of Mechatronics, Science Studies and Information, University of Technology, Kaunas, Lithuania

E-mail: carlo.menon@esa.int and info@VSFproject.com

Received 21 April 2006
Accepted for publication 26 July 2006
Published 17 August 2006
Online at stacks.iop.org/BB/1/52

Abstract
This paper presents and discusses a novel mechanism which was conceived taking inspiration from the micro-hydraulic system used by spiders to extend their legs. The mechanism has the potential to be used in future space applications, although the harsh space conditions, and in particular outgassing, should be carefully addressed in the design of a space-qualified model. The new system has one degree of freedom and is actuated by a pressurized fluidic system. The prototype, which has been designed, simulated, built and tested, is of compact size and presents a repeatable behaviour. The relation between pressure and rotation is approximately linear. The mechanism is suitable for a modular configuration in which several elastic joint modules are joined together. This modular configuration allows large rotations and does not increase the complexity of the actuation. A single module bends about 1.8° when the pressure of the working fluid is 1.2 MPa.

1. Introduction

Most animals have opposing muscles to articulate their joints: (6) flexors, which are used to bend the limbs, and (2) extensors, which straighten the joints. In spider legs, however, some joints do not have extensors as a peculiar hydraulic system is used for this purpose. Spiders have their legs directly attached to a main body called the prosoma as shown in figure 1. The prosoma, similarly to a pump, can increase the fluid pressure inside the spider by contracting and expanding. When the pressure is increased, the working fluid flows inside the limbs and extends some joints of the spider's legs.

This paper proposes and analyses a novel mechanism [1] which takes inspiration from spider limb joints and can be efficiently integrated in lightweight structures for space use. The paper is organized as follows: this section presents the motivations that led us to study inflatable systems for space applications and highlights the main challenges and inherent issues of this topic; section 2 investigates the spider hydraulic system and presents research results obtained so far; section 3 defines the problem that was studied; section 4 describes the novel mechanism, called Smart Stick, which was conceived; section 5 presents the design of the Smart Stick; section 6 presents the fabrication procedure used to obtain a prototype; section 7 discusses the modelling and the numerical simulations performed; section 8 describes the optical test bench used for the tests and presents the experimental characterization of the Smart Stick; section 9 presents, discusses and compares numerical and experimental results; section 10 proposes future improvements in the design and identifies the next development steps. Section 11 draws conclusions of the research performed and of the results obtained.

1.1. Inflatable systems

Space applications require structures, mechanisms and systems that are able to fulfil challenging tasks, while keeping their volumes and masses to a minimum. Gossamer structures are already a reality in the space field and research is

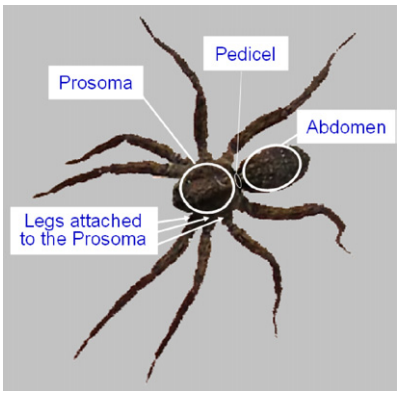

Figure 1. Spiders' subsystems of interest for the design of a bio-inspired fluidic mechatronic system.

giving new results thanks to the use of innovative materials and technologies. The Echo Balloon, the Inflatable Torus Solar Array Technology (ITSAT), the Inflatable Antenna Experiment (IAE) and the Inflated-Spherical-Wheel Rover are just a few examples of space inflatable still structures which have been tested in the past few years [3–9].

The use of inflatable mechanisms has some limitations due to the harsh space environment. Charged and high-energy particles, gas loss, solar ultraviolet and space radiation play an important role in the selection and development of inflatable materials.

In terrestrial use, pneumatic systems are often used for actuation. Pneumatic actuators are generally very fast but difficult to control. Often a 'bang–bang' control is used. Double-acting cylinders are advisable for differential pressure control. In this case, however, the complexity, cost and weight are increased. Muscle bio-inspired pneumatic actuators, first conceived for use in artificial limbs in the 1950–1960s [10], are now used and commercialized for anthroform bio-robotic arm development. An example of bio-inspired pneumatic actuators is the McKibben actuator [11]. This simple device consists of a braided sleeve, usually made of nylon wires, which contains a deformable bladder. Compressed air is used to inflate the bladder, and, since the strand is less extensible, an axial contraction of the actuator occurs. They are characterized by a high strength-to-weight ratio but the need for storage of compressed air in autonomous systems limits their use.

1.2. Hydraulic mechanisms

Literature on space inflatable systems that use liquid fluids as the inflating means is not as common as that for gas inflatable systems. Hydraulic mechanisms are generally not chosen for on-orbit/planets applications [5] for several reasons, e.g.:

1. liquid fluids outgas;
2. liquids are temperature sensitive;
3. liquids are heavier than gases;
4. hydraulic pumps induce vibrations and cavitations can occur.

Table 1. Planet characteristics.

	T (°C)			
	Range	Average	Pressure (kPa)	Composition
Mercury	[−173, 427]	179	None	K (31.7%)
Venus	[−44, 500]	464	9320	CO_2 (>96.4%)
Earth	[−69, 58]	7	101	N_2 (>78%)
Mars	[−140, 20]	−63	0.699–0.912	CO_2 (>95.3%)
Jupiter	[−163, /]	−121	Varies with depth	H_2 (>81%)
Saturn	[−191, /]	−130	Varies with depth	H_2 (>93%)
Uranus	[−214, /]	−205	Varies with depth	H_2 (>82%)
Neptune	[−223, /]	−220	Varies with depth	H_2 (>84%)
Pluto	[−240, −218]	−229	None	CH_3

The use of liquid fluids can, however, lead to new solutions and applications if the space hazards are carefully considered. The use of closed systems (no exchange with the environment) and low outgassing fluids characterized by low sensitivity to temperature changes can lead to the design of hydraulic space-qualified systems. Inflatable systems could also be designed by controlling the elasticity of the liquid tank. Miniaturized hydraulic mechanisms can be of particular interest. In fact, space applications do not generally require high force actuators, while mass must always be minimized. Taking advantage of their high strength-to-weight ratio, miniaturized hydraulic mechanisms could represent a compelling new approach.

1.3. The challenging space environment

A fundamental challenge for the use of inflatable space mechanisms is the space environment. Temperature range, pressure and atmospheric (if any) composition must be considered when a space mechanism is designed. Table 1 summarizes salient characteristics of some planets of the solar systems [4].

Outgassing and fluid leakage are important issues which must be considered during the design phase of space mechanisms. Considering, for instance, a probe on the Mars surface, the pressure is in the range 0.7–0.9 kPa, whereas on Venus there is a pressure of 9320 kPa. Mars has an average temperature of −63 °C whereas Venus is at about 464 °C, which could be prohibitive for conventional inflatable space architectures. The design of inflatable systems must therefore carefully take into account the surrounding operational environment.

In the framework of this study, which is at an early stage, the Earth environment was considered, because prototyping was considered a necessary step for the mechanism synthesis. Modifications must therefore be introduced when a different environment is considered.

2. Leg extension system in spiders

The legs of several arthropods (arachnids, diplopods, chilopods, pauropods) have joints that can be classified as hinge joints [13, 14]. The anatomical form of the joint often does not permit the presence of antagonistic extensors, which are often substituted by hydraulic systems. The empty

spaces in between muscles and skeleton are usually filled with haemolymph (spider's blood). This pressurized liquid is used as a means to pressurize the spider's joints. Thin channels supply haemolymph to peripheral segments through the leg.

In 1959, Parry and Brown carefully investigated spider legs and their pressurized mechanism. They showed experimentally that the active extension, which occurs at the hinge joints of the *Tegenaria* legs, is based on a hydraulic mechanism. They measured the internal pressure in the leg of an intact spider, established an empirical relation between the internal pressure and joint torque, and performed measurements of the actual torque developed when a spider accelerates a mass attached to its leg.

Many methods used to measure the leg inner pressure take advantage of the thin flexible articular membranes at the joints. For instance, Parry and Brown used a sleeve sealed over the leg. The pressure in the sleeve was slowly raised until the membrane collapsed [15]. Blickhan and Barth, in 1985, used a transducer with a tip smaller than the leg blood channels. The measurement system was mounted on freely moving spiders and also connected to several points of the hunting spider *Cupiennius salei* by means of tethers with negligible weight.

The mechanism for leg extension is now well documented for various spiders and whipscorpions [18, 19]. *Aphonopelma* have an inner pressure of about 5.3–8 kPa [22] and in walking *Mastigoproctus* the fluid arrives at a pressure up to 9 kPa [21]. In 1985, Blickhan and Barth measured up to 70 kPa on *Cupiennius salei* legs (130 kPa during autonomy). Several hypotheses have been supported by experiments to explain how the prosoma natural pump works [2, 15, 21–23].

Biologists were also able to measure the torque exerted by pressurized limb joints. It was shown that the torque increases approximately linearly with pressure [18]. The tibia–basitarsus joints of the tarantula *Aphonopelma* exert 20–74 mN mm when a pressure over the range 2.5–9.8 kPa is provided. Recent research reported high-resolution images, using transmission electron microscopy (TEM), which show cross sections of spider legs. By studying the legs of *Leiobunum nigripes*, Guffey [7], e.g., observed the presence of a single tendon, within a haemocoelic space, connecting the tarsal claw to the claw-flexing musculature of the tibia. The spider mechanism is also able to provide explosive force. High pressure can extend the rear legs, allowing spiders to jump [15, 16].

There have not been many attempts to design engineering models of spider joints. One of the most remarkable works was done by Schworer, Kohl and Menz [20]. Their mechanism was actuated by nitrogen and was able to lift a weight of 8.2 mN. The mechanism was built using extremely expensive equipment and processes (e.g. LIGA) suitable only for micro-systems.

3. Problem definition

Figure 2 shows a flow diagram of the mechanism to be designed. A command is given to an actuator, which compresses the working fluid. The fluid flows through a micro-pipeline and reversibly deforms an inflatable structure

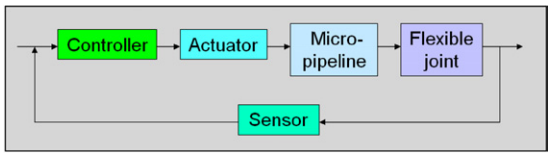

Figure 2. Flow diagram.

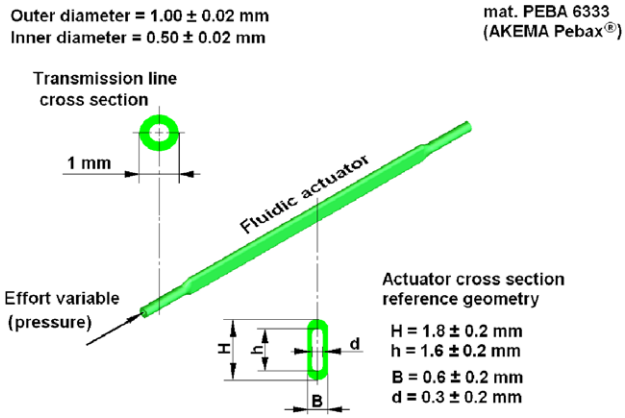

Figure 3. Fluidic actuator.

that produces a rotation of a flexible joint. The joint rotation is fed back by a sensor in order to correct the command.

The system should have a closed fluid system in order to reduce leaking problems and outgassing phenomena, which are compelling challenges for space mechanisms. There are no limitations on the working fluid, which could be a gas or a liquid.

The synthesis of the novel bio-inspired mechanism described in this paper focuses on the inflatable structure embedded in a flexible joint. The sensor unit and the mechanism used to compress the working fluid are not analysed at this stage. The mechanism is intended for operation in the space environment. However, the breadboard described in this paper was designed for terrestrial experiments.

Besides space and robotic applications, the proposed fluidic actuator could also be used in wearable equipment, e.g. smart bra [12].

4. Smart Stick

The novel conceived mechanism, called 'Smart Stick', is based on the use of a miniaturized tube (outside diameter 1 mm). The tube can be embedded into flexible structures to obtain integrated systems. Figure 3 shows the shape and dimensions of the miniaturized pipe obtained by plastic deformation. The part of the mini-tube having elliptical shape constitutes the 'fluidic actuator' of the system. Figure 4 shows the tube embedded in the 'Smart Stick' structure. The actuator acts upon hydraulic principles and the effects of the pressurization are stiffness variation and bending force generation in the structure.

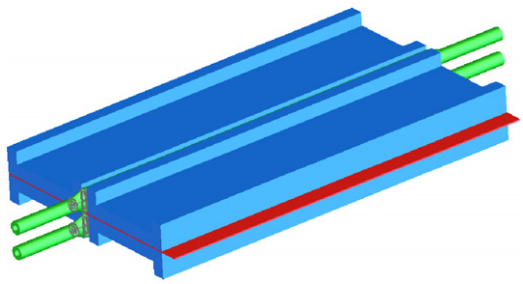

Figure 4. Elastic joint with two joint actuators.

The actuator manufacturing process can be repeated along the whole tube. The repeated process allows easy fabrication of a series of miniaturized fluidic actuators. By folding and deforming the mini-tube, mechanical connectors are avoided, making the system simple, reliable and light.

The design was conceived taking into account the manufacturing process and the robustness of the actuator. The case of a bi-phase fluid was also considered. The system is suitable for a closed loop control, which regulates the pressure p (effort variable) in the actuator.

5. Prototype design

The length of the actuators which were designed was 30 mm. The elliptical section of the mini-tube (see figure 3) was repeated along the tube every 15 mm. The tube was bent between each two elliptical sections in order to convey the working fluid to different joints. Figure 5 shows the rotation of a mechanism module induced by the deformation of the pressurized tube.

The pressurized tube expands, bending the inner metal foil along the bay. Eleven rigid spacers are glued to each side of the metal foil to ensure that each joint actuator works properly. In order to guarantee a controllable bending variation of the joint in both directions, the Smart Stick module is symmetrical with respect to its longitudinal axis.

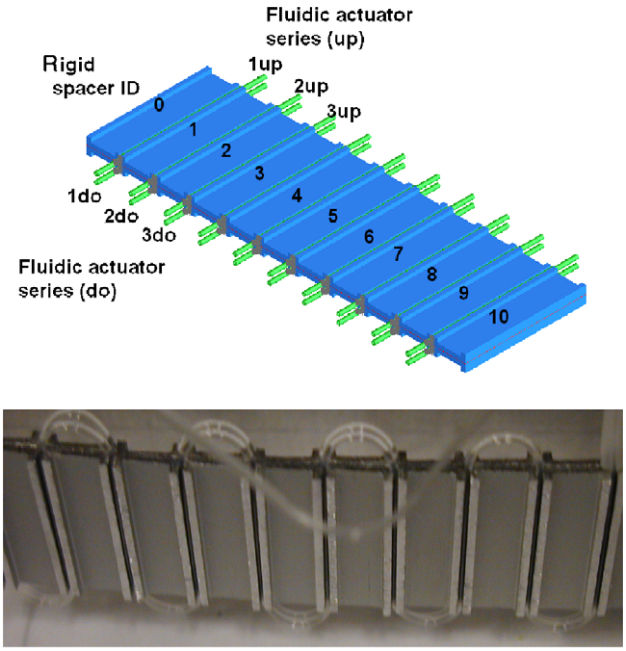

Figure 6. Prototype with two series of fluidic actuators and ten elastic joints.

Multiple modules of the Smart Stick can be embedded into one structure. Figure 6 shows both the design and the prototype which was built. This prototype has 10 elastic joints and 20 fluidic actuators. The action of actuators on the same side of the mechanism makes it bend with a constant curvature when no external loads are applied. By changing the position of simultaneously actuated joint actuators, different shapes of the Smart Stick can be obtained.

In order to assess the performance of the prototype, a custom-made pump syringe, used to increase the pressure of the working fluid inside the Smart Stick, was designed and built. Figure 7(A) shows the three-dimensional model of the pump syringe. A micrometre screw was used to regulate the

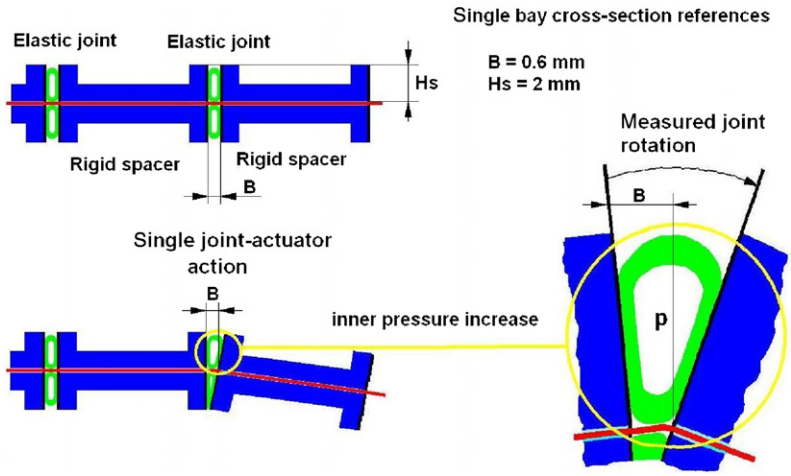

Figure 5. Smart Stick module, rigid spacer (blue), metal foil (red), fluidic actuator (green).

Table 2. Characteristics of the components of the Smart Stick system.

Component	Material	Dimensions
Flexible joint (foil)	X12CrNi177 (AISI 301) $E = 193$ GPa Density $= 8$ g cm^{-3} Tensile strength, ultimate $= 1280$ MPa Tensile strength, yield $= 965$ MPa Elongation at break $= 9\%$ Modulus of elasticity $= 193$ GPa	Length: 94 ± 0.1 mm Width: 30 ± 0.1 mm Thickness: 0.1 ± 0.004 mm
Spacers	Aluminium alloy Al–Mg series 6000 $E = 70$ GPa	'C' shape: (8 ± 0.1) mm $\times$ (2 ± 0.1) mm Thickness: 1 ± 0.05 mm
Mini-tubes (fluidic actuators)	AKEMA Poly Block Ammide (Pebax® 6333) $E = 276$ MPa	Outer diameter: 1 ± 0.02 mm Inner diameter: 0.5 ± 0.02 mm (see figure 3)

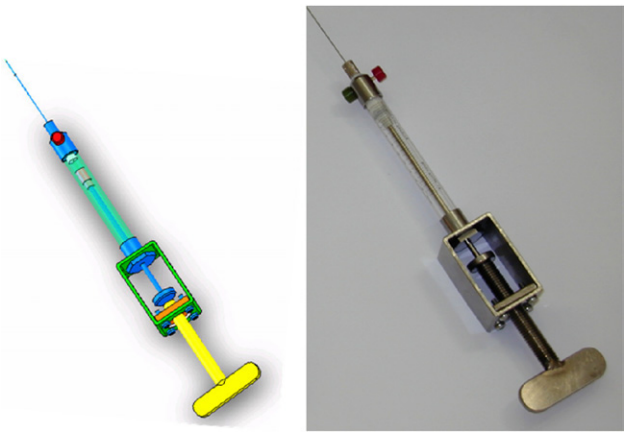

(A) (B)

Figure 7. Screw actuated pump syringe used during testing to increase the pressure of the working fluid.

pressure of the syringe which was sealed to the micro-tube of the Smart Stick. Figure 7(B) shows the screw actuated pump syringe built and then used for experimental tests.

6. Fabrication

The prototype was built using the components described in table 2. The procedure to fabricate the prototype is as follows:

1. The spacers, which had a 'C' shape, were accurately glued to a flexible joint (metallic foil).
2. The elliptical shape of the fluidic actuators was obtained by compressing the mini-tubes between two parallel surfaces.
3. The fluidic actuators were positioned between two consecutive spacers. Friction and compressive forces were sufficient to keep the actuators in their positions.

The data concerning the flexible joint, which is the element that mainly influences the linear elastic behaviour and stiffness of the Smart Stick, were experimentally tested by using the set-up shown in figure 8.

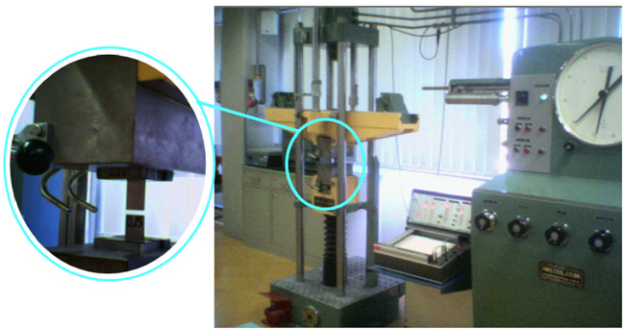

Figure 8. Set-up for the characterization of the flexible joint (metal foil) of the Smart Stick.

7. Smart Stick modelling

The performance of the Smart Stick was numerically assessed by modelling the mechanism. Nonlinear numerical simulations were performed using Marc, a finite-element method code. Figure 9 shows the model of one Smart Stick module with just one fluidic actuator: an elliptical tube (green) is set between two spacers (blue) which are attached by a flexible joint (red). The mesh of the model is also shown in figure 9 (white).

Positions of the nodes on the right-hand side of the model were fixed (black lines). Contact constraints were imposed at the tube/spacer and tube/joint interfaces. Nodes between the spacers and the flexible joint were merged. The two orange dots in figure 9 represent two nodes shared by the elliptic tube and the spacers. A constant pressure was imposed inside the elliptical tube. Figure 10 shows the deformation of the fluidic mechanism when the tube is pressurized.

A sensitivity analysis was performed in order to understand the critical parameter of the design. Dimensions and material properties of the flexible joint (red in figure 9) play a fundamental role, by defining the relation between rotation of the joint and inner pressure in the tube. The linear behaviour of the flexible joint in large displacement ranges implies a linear behaviour of the mechanism.

A complete model including fluidic actuators on both sides of the flexible joint was also designed. Figure 11 shows the deformation of a Smart Stick with six modules. The total

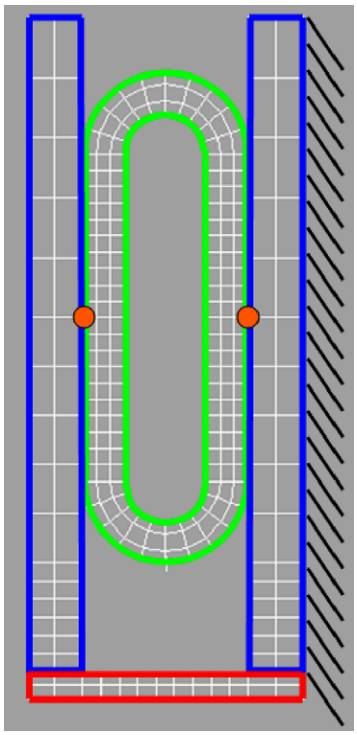

Figure 9. Two-dimensional model.

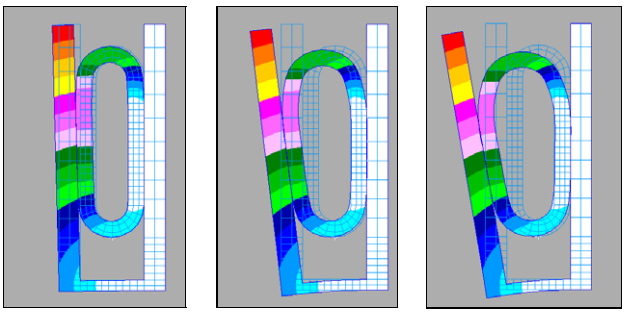

Figure 10. Visual deformation of one module.

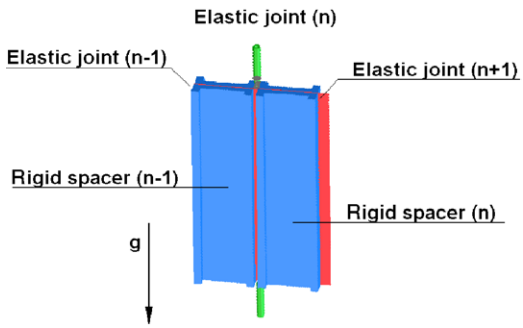

Figure 12. Elastic joint in vertical position with only one fluidic actuator in the bay.

rotation of the system increases linearly with the number of the modules used. In this complete module, the fluidic actuators at the bottom of figure 11(A) act as antagonist muscles. As a not negligible force is requested to compress them (see squeezed antagonist fluidic actuators in figure 11), the rotation of the Smart Stick is expected to be reduced. On the other hand, antagonist actuators allow negative rotations of the system as shown in figure 11(B).

8. Experimental characterization and optical test bench

A Smart Stick module was tested in order to obtain the relation between fluid pressure and joint rotation (water was used as the working fluid). An empirical model is useful to predict the behaviour of the Smart Stick in the control algorithm. Figure 12 shows the elastic joint in vertical configuration obtained by fixing the rigid spacer $(n-1)$. A vertical configuration was used to reduce the influence of the gravitational force.

Gravitational forces do not cause appreciable deformations as the inner metal foil has high flexural stiffness around an axis perpendicular to the axis of joint rotation. During the experiment, no external loads were applied to the elastic joint (except gravity).

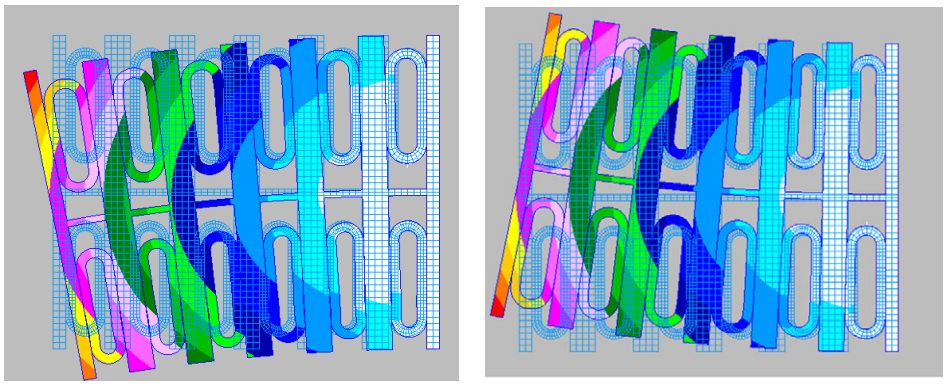

(A) (B)

Figure 11. Model of six Smart Stick modules. Colours give a qualitative value of the deformations.

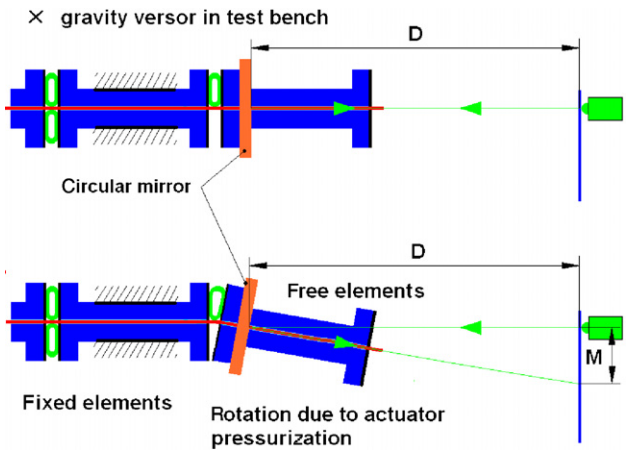

Figure 13. Sketch of the test bench.

An optical test bench, which is schematically shown in figure 13, was used to perform the experimental characterization. The first pair of rigid spacers was fixed and referred to the incoming ray trace. Figure 13 shows the circular mirror fixed on the second pair of rigid spacers. In the nominal horizontal position, the mirror is perpendicular to the rays coming from a laser source fixed to a screen frame. Depending on the mirror angle, the reflected ray trace moves on the screen, by a measured distance M.

8.1. Test bench overall dimensions

The distance (D) between the mirror and the laser source (see figure 13) is 2 m. The uncertainty associated with D, with a level of confidence of 68.3%, is $\delta_D = 1.5$ mm. The uncertainty in the direct measurement of deflection distance (M), with a level of confidence of 68.3%, is $\delta_M = 0.5$ mm.

The rotation of the Smart Stick module was computed by the following equation:

$$\theta = \frac{1}{2}\,\mathrm{arctg}\left(\frac{M}{D}\right). \tag{1}$$

For small angles, the previous equation can be simplified:

$$\theta \approx \frac{1}{2}\left(\frac{M}{D}\right). \tag{2}$$

The uncertainty δ_θ associated with the angle θ can be computed as follows:

$$\delta_\theta = f(\theta, M) = \sqrt{\left[\left(\frac{\partial\theta}{\partial M}\right)\cdot\delta_M\right]^2 + \left[\left(\frac{\partial\theta}{\partial D}\right)\cdot\delta_D\right]^2}. \tag{3}$$

Substituting equation (2) in equation (3) yields:

$$\delta_\theta = \sqrt{\left[\left(\frac{1}{2}\frac{1}{D}\right)\cdot\delta_M\right]^2 + \left[\left(-\frac{1}{2}\frac{M}{D^2}\right)\cdot\delta_D\right]^2}. \tag{4}$$

Considering the assumption of the model and additional variables that were neglected, the uncertainty i_θ of the angle θ can be assumed to be equal to 0.3° (99.7% level of confidence). Figure 14 shows the experimental set-up (two fluidic actuators are represented).

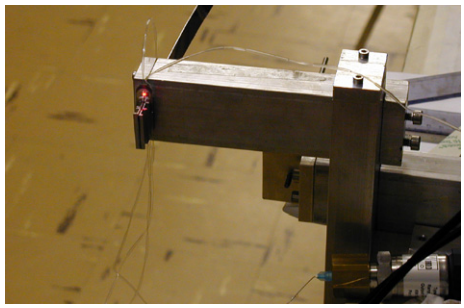

Figure 14. Elastic joint in test bench.

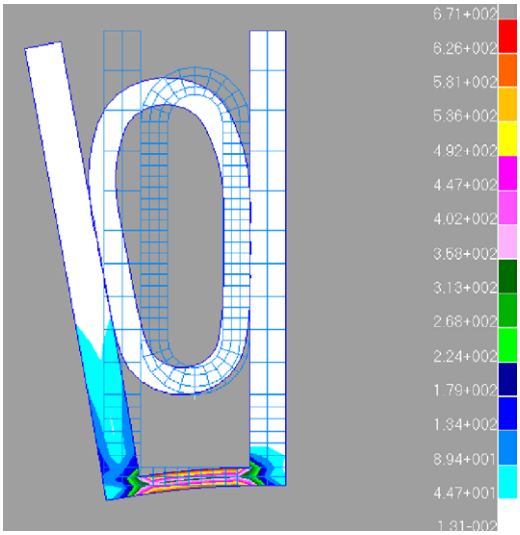

Figure 15. Stresses caused by the deformation of one single fluidic actuator module induced by a pressure of 1.2 MPa. In the legend, the values are in MPa.

The uncertainty in the effort variable p (pressure of the working fluid) was $i_p = 0.013$ MPa (99.7% level of confidence) as declared in the calibration certificate of the pressure gauge which was used.

9. Numerical and experimental results

Numerical simulations were extremely useful to predict the performance and accurately define the geometry of the Smart Stick. Figure 15 shows the stresses in a single fluidic actuator module due to a deformation induced by a pressure of 1.2 MPa. Using the von Mises criterion, the maximum stress was 671 MPa localized in the flexible joint. This value is below the tensile yield strength of the AISI 301 austenitic stainless steel foil (965 MPa). The use of a thinner flexible joint is believed to increase the structural stresses while increasing the Smart Stick rotation for a fixed fluid pressure.

Different quasi-static simulations of a single module of the Smart Stick were performed while changing the pressure value inside the fluidic actuator. Dimensions and material described in section 5 were used. The numerical model foresees good

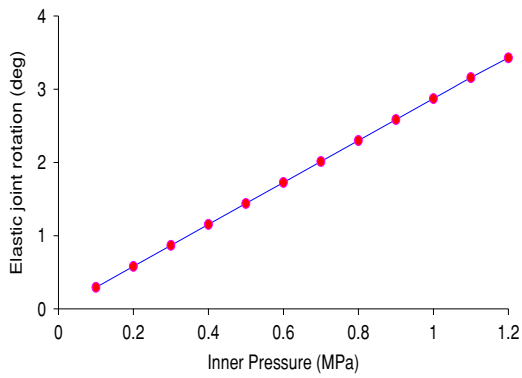

Figure 16. Numerical prediction of one Smart Stick module with only one fluidic actuator. Red dots: experimental results. Blue line: linear fitting curve.

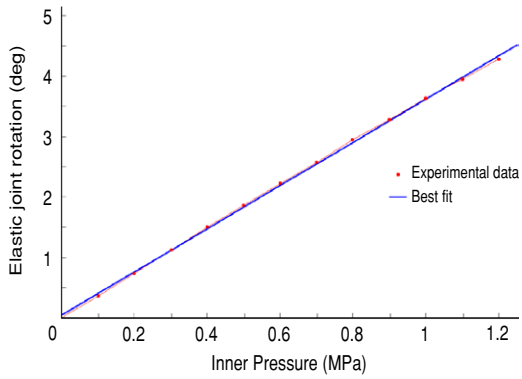

Figure 17. Experimental results of one Smart Stick module with only one fluidic actuator. Red line: experimental results. Blue line: linear fitting curve.

performance of the system as presented in figure 16. This figure shows that the rotation of a module is linearly changing with the pressure inside the fluidic actuators (the red dots represent single quasi-static numerical simulations; the blue line is a fitting curve).

Several experimental tests were also performed using the Smart Stick prototype in order to characterize its behaviour. Figure 17 shows that the rotation of the joint can be approximated with a linear function (blue line). Figure 17 concerns the use of one module of the Smart Stick having only one fluidic actuator embedded in the system. Figure 18 shows experimental results for eight cycles using the same joint module. A fitting of the experimental data was performed in order to obtain an empirical equation that could be used for control purposes:

$$\theta = \theta(p) = 3.57p + 0.13, \tag{5}$$

where the angle is in degrees and the pressure in MPa. The uncertainty (99.7% level of confidence) associated with the slope of the function is $\pm 0.13^\circ$ MPa^{-1} and that associated with the intercept is $\pm 0.24^\circ$.

Figures 17 and 18 show the behaviour of the Smart Stick that was correctly predicted by the numerical simulations (figure 16). Comparison of numerical end experimental tests proves both the correctness of the model and the quality of the

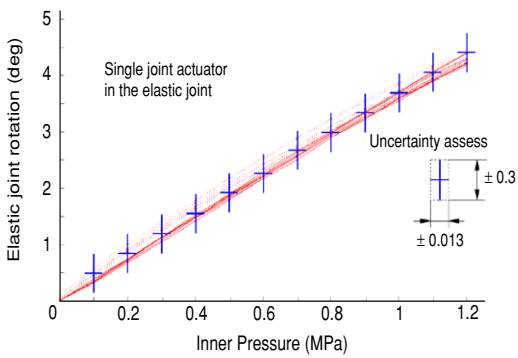

Figure 18. Multiple cycles of one Smart Stick module (only one fluidic actuator).

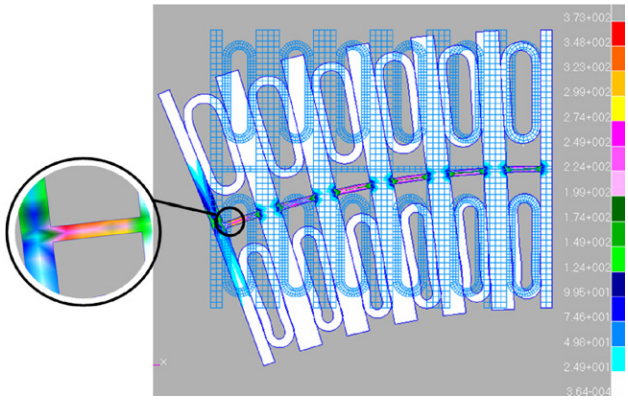

Figure 19. Stresses caused by the deformation of the Smart Stick induced by a pressure of 1.2 MPa. In the legend, the values are in MPa.

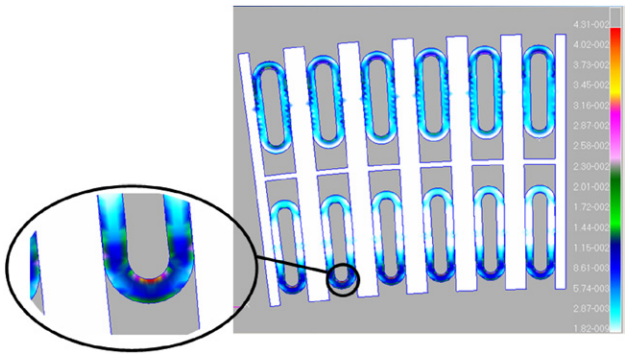

Figure 20. Strains caused by the deformation of the Smart Stick induced by a pressure of 1.2 MPa. In the legend, the values are in percentage.

experimental set-up. In addition, figures 17 and 18 confirm the high performance of the Smart Stick breadboard and show its potential for future applications.

Numerical predictions of a complete Smart Stick were also estimated by means of numerical simulations. Stresses induced on modules made of counteracting fluidic actuators are shown in figure 19. In this case, the presence of the antagonist actuators reduces the bending stresses. The maximum stress pick is still concentrated in the flexible joint and measures

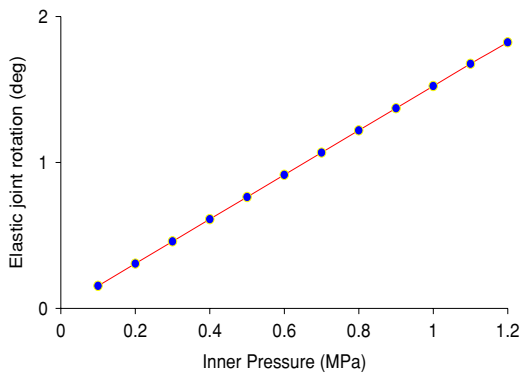

Figure 21. Numerical prediction of one Smart Stick module with only one fluidic actuator. Blue dots: experimental results. Red line: linear fitting curve.

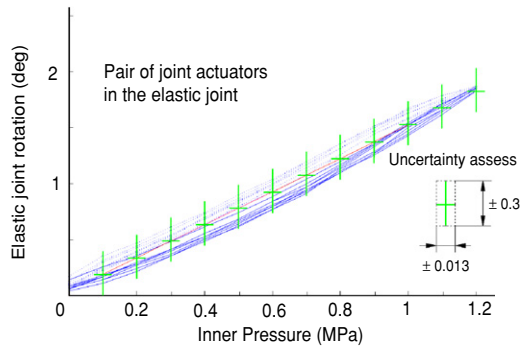

Figure 22. Multiple cycles of one Smart Stick module (two fluidic actuators).

373 MPa. Figure 20 shows that, for the same pressure loads, the maximum strain is reached by the compressed fluidic actuators. The maximum value is about 4%, which is in the range of deformations allowed by the material used for the micro-tubes (AKEMA Poly Block Ammide).

Quasi-static simulations of a single Smart Stick module equipped with opposing fluidic actuators were also performed and figure 21 shows the results. The system still has a linear behaviour which is guaranteed by the linear elasticity of the flexible joint. Compared to the case shown in figure 16, the deformation predicted by figure 21 is lower as an additional force is in this case required in order to compress the antagonist fluidic actuator.

This predicted performance was validated by experimental tests carried out considering a module of the Smart Stick equipped with two antagonistic fluidic actuators. Figure 22 shows the experimental results of eight pressurization/depressurization cycles. A fitting of the experimental data was performed in order to obtain an empirical equation that could be used for control purposes:

$$\theta = \theta(p) = 1.49p + 0.04, \tag{6}$$

where the angle is in degrees and the pressure in MPa. The uncertainty associated with the slope of the function is $\pm 0.11^\circ$ MPa^{-1} and uncertainty associated with the intercept is $\pm 0.15^\circ$.

The consistency of the numerical prediction shown in figure 21 and the experimental results of figure 22 confirms the reliability of both the numerical model and the experimental set-up.

10. Future improvements and designs

In order to increase the performance of the Smart Stick, a careful selection of the material employed is needed. The use of aerogels and lighter and more flexible materials for the spacers is being considered. Improvement in the design will focus on multiple parallel mini-tubes which can bring more flexibility to the system.

The fundamental next step necessary to obtain a complete mechatronic breadboard for space applications will be the realization of the multi-module Smart Stick incorporating a closed fluid loop. Figure 23 shows a sketch which presents the concept idea of two symmetric closed fluid loops in a spider inspired configuration. In this figure, the controller sends the commands to an actuator mechanism that squeezes an expandable reservoir. The pressure of the working fluid, which is confined inside a closed loop, is thus increased. A micro-pipe links the reservoir to the Smart Stick which changes

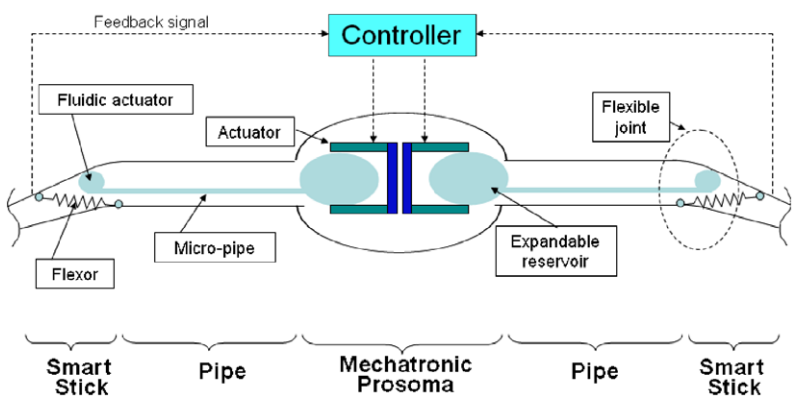

Figure 23. Sketch of a closed fluid loop.

its shape according to the pressure values. The rotation of the flexible joint, in which the Smart Stick is integrated, is measured by embedded sensors that feed back the signal to the controller.

The use of a closed fluid loop, which allows overcoming leakage and outgassing issues, is considered to be a critical point for a successful hydraulic space mechanism. Future work will be focused on the development of a complete closed loop mechatronic system and particular attention will be paid to the actuation system. This could include smart materials such as piezoelectric materials, shape memory alloys and electro-active polymers [17, 24]. In particular, dielectric electro-active polymers have promising characteristics for this application as they exert considerable forces in a wide range of large deformations and can be space qualified. Magneto-restrictive fluids will also be evaluated in order to improve the torque performance of the system.

11. Conclusions

A novel flexible joint with an embedded fluidic system is presented in this paper. The novel mechanism is inspired by the joints and the hydraulic closed system of spiders. The proposed mechanism can be fabricated using traditional and inexpensive processes and methodologies. The modularity of the mechanism can be used to design joints for large displacements. The system was numerically simulated in order to appropriately design the geometry and to predict its quasi-static characteristics. A miniaturized prototype was also built and tests were performed by using an optical test bench. Numerical and experimental results are consistent and show the feasibility of the design. Improvements of the system are also suggested and a closed fluid loop configuration is proposed for future investigations.

Acknowledgments

The work was carried out thanks to NATO grant awarded to Cristian Lira (grant no NATO-CNR 215.36). The authors also thank Susanna Valpreda for her valuable support in the bibliographic review, VICI AG International for providing components of the screw actuated pump syringe, Mario Vannin for the characterization of the flexible metal foil and Devis and Romeo Facchin for their support in the manufacturing part.

References

[1] Menon C and Lira C 2006 Spider-inspired embedded actuator for space applications *AISB'06—Adaptation in Artificial and Biological Systems (Bristol)*

[2] Anderson J F and Prestwich K N 1975 The fluid pressure pumps of spiders (Chelicerata, Araneae) *Z. Morphol. Tiere* **81** 257–77

[3] Bar-Cohen Y 2000 Electroactive polymers as artificial muscles—capabilities, potentials and challenges *Robotics 2000 and Space 2000 (Albuquerque, NM, 28 February–2 March)*

[4] Barik M E 2000 *Planetary Handbook* (Cambridge: Cambridge University Press)

[5] Benaroya H, Bernold L and Chua K M 2002 Engineering, design and construction of lunar bases *J. Aerospace Eng.* **15** 33–45

[6] Blickhan R and Barth F G 1985 Stains in the exoskeleton of spiders *J. Comp. Physiol.* **157** 115–47

[7] Guffey C, Townsend V R Jr and Felgenhauer B E 2000 External morphology and ultrastructure of the prehensile region of the legs of *Leiobunum nigripes* (Arachnida, Opiliones) *J. Arachnol.* **28** 231–6

[8] Kitagawa A, Tsukagoshi H and Segawa M 2000 Proposal of a connective type active hose with many degrees of freedom for the rescue operation *6th Triennial Int. Symp. on Fluid Control, Measurement and Visualization (Sherbrooke, Canada, 2000)*

[9] Jenkins C H M 2001 Gossamer spacecraft: membrane and inflatable structures technology for space applications *Prog. Astronaut. Aeronaut.* **191** 481–501

[10] Knight R and Nehmzow U 2002 Walking robots: a survey and a research proposal *Technical Report* CSM-375 (University of Essex)

[11] Chou C P and Hannaford B 1994 Static and dynamic characteristics of McKibben pneumatic artificial muscles *Proc. IEEE Int. Conf. on Robotics and Automation (San Diego, CA, May 1994)*

[12] Lira C, Angrilli F and Debei S 2002 Variable structure fabric and uses for it *Patent Document* WO02099172

[13] Manton S M 1958 Evolution of arthropodan locomotory mechanisms: part 6 *J. Unn. Soc. (Zool.)* **43** 488–556

[14] Manton S M 1958 Hydrostatic pressure and leg extension in arthropods *Ann. Mag. Nat. Hist. (Series 13)* **1** 161–82

[15] Parry D A and Brown R H J 1959 *The Hydraulic Mechanism of the Spider Leg* (Department of Zoology, University of Cambridge

[16] Parry D A and Brown R H J 1959 The jumping mechanism of salticid spiders *J. Exp. Biol.* **36** 654–64

[17] Rossi D, Carpi F, Jeronimidis G, Gaudenzi P, Tralli A, Zolesi V and Ayre M 2004 *Electroactive Polymers for Actuation and Sensing in Space Applications (IAC, AIAA, Vancouver, Canada)*

[18] Sensenig A T and Shultz J W 2003 Mechanics of cuticular elastic energy storage in leg joints lacking extensor muscles in arachnids *J. Exp. Biol.* **206** 771–84

[19] Sensenig A T and Shultz J W 2004 Elastic energy storage in the pedipalpal joints of scorpions and sun-spiders (Arachnida, Scorpiones, Solifugae) *J. Arachnol.* **32** 1–10

[20] Schworer M, Kohl M and Menz W 1998 Fluidic microjoints based on spider legs *Conf. on New Actuators (Bremen)*

[21] Shultz J W 1991 Evolution of locomotion in Arachnida: the hydraulic pressure pump of the giant whipscorpion, *Mastigoproctus giganteus* (Uropygi) *J. Morphol.* **210** 13–31

[22] Stewart D M and Martin A W 1974 Blood pressure in the tarantula, *Dugesiella hentzi J. Comp. Physiol.* **88** 141–72

[23] Wilson R S and Bullock J 1973 The hydraulic interaction between prosoma and opisthosoma in *Amaurobius ferox* (Chelicerata, Araneae) *Z. Morphol. Tiere* **74** 221–30

[24] Menon C, Ayre M and Ellery A 2006 Biomimetics: a new approach for space systems design *ESA Bull.* **125** 20–6